Distributed Tensor Network Library for Quantum Computing Emulation

Jakub Adamski
EPCC
University of Edinburgh
Edinburgh, United Kingdom
0009-0000-5221-2070

Oliver Thomson Brown
EPCC
University of Edinburgh
Edinburgh, United Kingdom
0000-0002-5193-8635

arXiv:2505.06119v1 [cs.DC] 9 May 2025

***Abstract*—Tensor networks offer an adaptable and efficient approach to emulation of quantum computers. Their usage relies on partitioning circuits into small tensors, which are contracted together to form the final result. While this approach intends to minimise the problem size, exceeding the locally available memory is sometimes unavoidable due to the exponential nature of quantum systems. Most HPC tensor network packages tackle this issue with a procedure called circuit slicing, which distributes the entire network onto multiple ranks, recombining it back when necessary. In this study, we present a novel alternative approach, where individual tensors are both broadcast and scattered to harness multiple levels of parallelism. The technique is abstracted behind a fixed distribution pattern, and actualised in a new portable tensor network library, QTNH, built on top of MPI and ScaLAPACK. We showcase its capabilities on ARCHER2, by emulating two well-known algorithms – the Quantum Fourier Transform and Random Circuit Sampling. This is accomplished by leveraging the implemented operations to realise various contraction strategies, including a unique distributed MPS tensor factorisation approach. We thus demonstrate that our library can be used to advance the accuracy of quantum emulation, while offering a simple and flexible interface to tensor distribution.**

***Index Terms*—high performance computing, quantum computing, tensors, cluster computing, software**

I. Introduction

Quantum computing is an emerging computational paradigm that has been growing in popularity in the latest decade – promising polynomial to exponential speedups to certain problems, such as spatial search, order finding, or eigenstate optimisation [1]–[3]. With recent developments in hardware and error-correction, it is projected that the era of useful quantum devices is due to start in a matter of years [4]. However, the technological improvements lead to an amplified need for classical emulation, which provides a controlled environment to model and analyse quantum behaviour. This is an exponentially hard task – while a classical register only stores one bitstring at a time, its quantum counterpart can simultaneously hold all possible combinations. Hence, classical emulation of quantum computers is a perfect fit for large HPC clusters [5].

Generally, a quantum circuit can be expressed in the language of *tensor networks*, which offers a universal and flexible approach to emulation [6]. This is attained by performing repetitive pairwise contractions – tensor equivalents to matrix multiplication. The benefit of this technique is adaptability, as the contractions can follow in any order, optimised either for speed or memory usage [7]. In addition, there are other tensor operations that facilitate representation of quantum information, e.g. singular value decomposition (SVD), adopted to compress/truncate tensor dimensions. This makes tensor networks particularly well-suited for emulation of noisy systems, where accuracy and precision are expected to decline [8].

In the context of HPC, larger tensor networks may entail significant memory overheads at some point during contraction, which is common in areas like quantum computing or chemistry, where the state size is exponential in the number of qubits. While many available tools are sequential and rely on minimising the memory usage [9], [10], a few libraries remedy that by offering a way to distribute the tensors. This can be attained by *slicing* the main network into smaller subnetworks and contracting the segments in parallel [11]–[13]. However, such an approach is based on the distribution and contraction of the entire network, and doesn't focus on individual tensors. Moreover, an external linear algebra library might need to be manually called, which impacts usability [11].

In this paper, we present **Quantum Tensor Network Hub (QTNH)** – an adaptive and portable distributed tensor network library that employs a distinct distribution pattern designed to scatter individual tensors, while continuing to harness the parallelism of independent contractions. QTNH mainly targets emulation of quantum computing, providing multiple strategies established on top of tensor networks, from statevector evolution to matrix product states. The underlying linear algebra routines are bound to ScaLAPACK to enable large-scale tensor operations, while the distribution and element exchange is handled with MPI. The library is currently aimed for large CPU-based high-performance clusters, such as ARCHER2, but in the future, it could be augmented to support GPU-offloading for faster local computation [14].

It is important to highlight that QTNH is not made with primary focus on performance, as the main reason to scale up the emulations is to increase the size and/or accuracy of the related system. In fact, the parallel efficiency of operations on distributed general tensor networks is often remarkably low, as a result of frequent data exchange with irregular communication patterns, and costly routines like the SVD [15].

Nevertheless, as the quality of emulated hardware goes up, so does the simulation complexity, and the need to leverage distributed systems remains.

This paper is divided into five further parts. In section II, we outline the relevant topics, such as quantum computing, algorithms and circuits, approaches to quantum emulation and tensor networks. We also point towards other available HPC libraries. Section III examines the implementation details and considerations behind QTNH, and sets up the experimental framework to demonstrate the library's capabilities. These are showcased and evaluated in section IV, which helps pinpoint primary target use-cases, and identify current limitations, while section V suggests improvements to address the shortcomings. Finally, section IV concludes the study.

II. Background

In this chapter, we briefly cover the applicable ideas and background material linked to the contents of this paper – i.e. basics of quantum computing and emulation techniques. For more in-depth background, a detailed introduction to quantum computation is provied in [16], while the relevant tensor network concepts are explained in [17] and [18].

A. Quantum computing

Just like classical computing is based on bits, quantum computing uses quantum bits, called *qubits* in short. A fundamental difference from their classical counterpart is that a qubit can store a *superposition* of both binary 0 and 1 values. To denote this, we use *Dirac notation*:

$$|\psi\rangle = a\,|0\rangle + b\,|1\rangle$$

The complex coefficients a and b are related to the probability of measuring corresponding values by the squared modulus function. This imposes a constraint that $|a|^2 + |b|^2 = 1$.

Multiple qubits can be combined into a *quantum register* via *tensor product* operation, e.g. $|\psi_1\rangle \otimes |\psi_2\rangle = a_1 a_2\,|00\rangle + a_1 b_2\,|01\rangle + b_1 a_2\,|10\rangle + b_1 b_2\,|11\rangle$. This preserves the probability constraint, i.e. all coefficients squared still add up to one. In general, we can write:

$$|\Psi\rangle = \sum_{i=0}^{2^n-1} \psi_i\,|i\rangle$$

to represent a register with n qubits. The integer states $|i\rangle$ are equivalent to decimal notation of binary states.

A quantum register remains in superposition until it is *measured*. After the measurement, it collapses to whatever value is observed, and the probability is renormalised. This also applies to *partial measurements*, where only a subset of qubits are observed. For instance, in a state $\psi_0\,|00\rangle + \psi_1\,|01\rangle + \psi_2\,|10\rangle + \psi_3\,|11\rangle$, if the first qubit is measured as $|0\rangle$, the state collapses into $\psi_0'\,|00\rangle + \psi_1'\,|01\rangle$, where the coefficients are renormalised so that the probability constraint is preserved:

$$\psi_0' = \frac{\psi_0}{\sqrt{|\psi_0|^2 + |\psi_1|^2}} \quad \text{and} \quad \psi_1' = \frac{\psi_1}{\sqrt{|\psi_0|^2 + |\psi_1|^2}}$$

A quantum state in the register can be modified with *quantum gates*, which describe how new elements are computed based on some linear combination of the old elements. Therefore, as the state can be treated as a vector of 2^n elements, a general gate is a $2^n \times 2^n$ matrix. However, in most cases, quantum gates act on only a subset of all qubits, so instead they use $2^k \times 2^k$ elements for a k-qubit gate.

Another property of quantum registers is *entanglement*. This occurs when the register can no longer be represented as a tensor product of individual qubits, which can happen after a two (or more) qubit gate is applied. For instance, the state $\frac{1}{\sqrt{2}}(|00\rangle + |11\rangle)$ is entangled. In general, a quantum state can be split into two parts using the following relation:

$$|\psi\rangle = \sum_i \lambda_i \left|\phi_i^{(A)}\right\rangle \left|\phi_i^{(B)}\right\rangle$$

where A and B label the subsystems. This is called *Schmidt decomposition*, and we say the subsystems are entangled if there are multiple terms in the summation. Interestingly, this decomposition is equivalent to a singular value decomposition (SVD) of the original state reshaped as a matrix.

B. Quantum algorithms

Quantum circuits implement quantum algorithms, designed for solving specific tasks. Some algorithms are variational, i.e. they use variable coefficients for finding a global minimum to a given cost function. However, this usually requires a large number of runs with significant processing overheads, which is costly to emulate. Hence, in this paper, we focus on algorithms that don't rely on re-runs, so that most information can be derived from the output state. More specifically, we selected two problems – quantum Fourier transform and random circuit sampling, which can be distinguished by the level of entanglement they add to the input state.

Quantum Fourier transform (QFT) is a quantum version of the discrete Fourier transform. Its action performs the following transformation between elements of the input state $|x\rangle$ and the output state $|y\rangle$:

$$y_k = \frac{1}{2^n} \sum_{j=0}^{2^n-1} \exp\left(2\pi i \cdot \frac{jk}{2^n}\right) \cdot x_j$$

In the equation above, i is an imaginary number, and not a parameter. The coefficients x_j/y_k correspond to j-th/k-th elements of the input/output state. This can be implemented with a circuit consisting of Hadamard gates and controlled phase gates:

$$\hat{H} = \frac{1}{\sqrt{2}}\begin{pmatrix} 1 & 1 \\ 1 & -1 \end{pmatrix}, \quad \hat{CZ}(\theta) = \begin{pmatrix} 1 & 0 & 0 & 0 \\ 0 & 1 & 0 & 0 \\ 0 & 0 & 1 & 0 \\ 0 & 0 & 0 & e^{i\theta} \end{pmatrix}$$

The QFT is used as an important routine of other algorithms, for example *quantum phase estimation*, which is used for the famous Shor's algorithm [2]. An important feature of this algorithm is that it doesn't introduce much new entanglement [19]. An example QFT diagram is shown in Fig. 1. The swap gates

at the end are required to preserve the qubit ordering, but are often omitted when the QFT is a part of larger algorithms.

Random circuit sampling (RCS) is a benchmarking algorithm introduced by Google in their quantum supremacy paper [20]. Its main goal is to apply random gates to generate a highly entangled quantum state, which is then sampled from. The following three gates are randomly selected for each qubit at every layer:

$$\hat{X}^{1/2} = \frac{1}{\sqrt{2}}\begin{pmatrix} 1 & -i \\ -i & 1 \end{pmatrix}, \quad \hat{Y}^{1/2} = \frac{1}{\sqrt{2}}\begin{pmatrix} 1 & -1 \\ 1 & 1 \end{pmatrix},$$
$$\hat{W}^{1/2} = \frac{1}{\sqrt{2}}\begin{pmatrix} 1 & -\sqrt{i} \\ \sqrt{-i} & 1 \end{pmatrix}$$

In addition, every layer is ended by a series of two-qubit entangling gates applied in a repeated pattern. The gates are assumed to lie on a square grid, and the entangling operations connect nearest neighbours either up/down or left/right to each qubit, in one of four patterns – A, B, C or D, which are then applied to every layer in a cyclic order $ABCDCDAB$. The entangling gates have the following form:

$$f\hat{Sim} = \begin{pmatrix} 1 & 0 & 0 & 0 \\ 0 & 0 & -i & 0 \\ 0 & -i & 0 & 0 \\ 0 & 0 & 0 & e^{-i\pi/6} \end{pmatrix}$$

An example RCS circuit is shown on Fig. 2. The output bitstring should follow a Porter-Thomas distribution, which is difficult to reproduce classically. As a result, the quantum computer "solves" a task that a classical computer would struggle with. This is mainly due to the two-dimensional connectivity between qubits, which introduces high entanglement.

C. Traditional emulation strategies

Emulating quantum computers is a complex problem, as the state space grows exponentially with the number of qubits. As a result, to fully represent an arbitrary state, it is unavoidable to store all 2^n elements in memory. The state is then evolved by applying gates as matrices. An arbitrary gate would need 4^n matrix elements, but in practice, common gates rarely exceed 2 qubits, and therefore require no more than 16 distinct elements. In addition, a vast majority of elements are zero, and large unitaries have a uniform structure. Hence, it is possible to calculate the required elements and their positions on-demand, making the memory footprint vanishingly small compared to the statevector. However, the time complexity of applying a

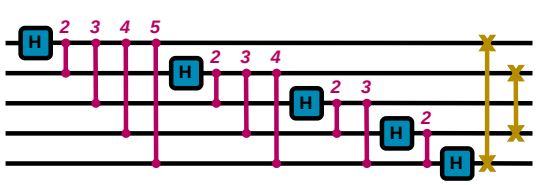

Fig. 1. Example 5-qubit QFT diagram. Magenta lines correspond to controlled phase gates, where the phase angle is $\phi = \frac{2\pi}{2^k}$, and k is given above the gate.

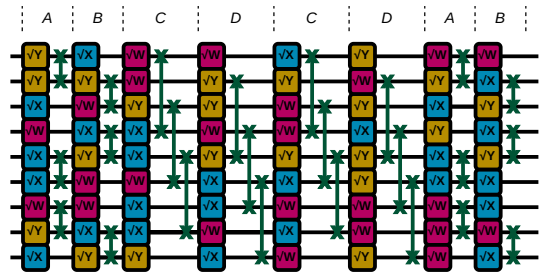

Fig. 2. Example RCS diagram of a quantum processor with 3×3 qubit layout. Each layer has a sequence of random gates (selected from $\hat{X}^{1/2}, \hat{Y}^{1/2}, \hat{W}^{1/2}$), and a sequence of two-qubit fSim gates (iSWAP followed by a controlled phase shift by $\frac{\pi}{6}$) according to one of four patterns (A, B, C, D). The layer pattern sequence used is $ABCDCDAB$.

single gate is still 2^n, as in a general case, all elements need to be updated. This method is called the **Schrödinger approach**.

To avoid exponential memory prerequisites, an alternative method can be used. Let us suppose that we are only interested in one out of 2^n final state elements. It is possible to calculate this element by following all possible paths that reach it and adding the contributions from each path. This is inspired by *Feynman paths* from quantum mechanics, and is thus called the **Feynman approach**. It turns out that each gate increases the number of possible path by a factor of 2^q, where q is a number of qubits being acted on. Therefore, for at most 2-qubit gates, the total time complexity is 4^d, where d is the *depth* of the circuit, i.e. the number of gates. Meanwhile, the memory footprint is vanishingly small, as only one element is updated. Unfortunately, the depth of the circuit is usually much higher than the register size, which means this approach is intractable for a majority of real-life circuits.

The third option is to use the **Schrödinger-Feynamn approach**, which combines both methods to reduce memory consumption at much lower runtime complexity. The idea is to split the state into two or more subsystems, each being emulated using the Schrödinger approach within itself, while the connecting gates are treated as paths, and contribute to the runtime multiplicatively.

D. Tensor networks

All the techniques above are called **statevector approaches**, as they involve directly evolving elements of the state. However, there is an alternative based on **tensor networks**. Here, the entire circuit is treated as a network of tensors, which can be contracted (i.e. multiplied) in any order.

Tensor are equivalents of multi-dimensional arrays, with the *rank* specifying how many dimensions are in a tensor. They can be visualised by a box with multiple lines pointing out, which are also called *indices*, where the number of indices is the same as the tensor rank. Each index has a *dimension*, which is the number of labels at a given index used to identify the elements. Every combination of labels at each index points at a *tensor element* – a complex number in the context of quantum computing. Therefore, for a rank r tensor, with index dimensions of $(d_0, d_1, \ldots, d_{r-1})$ has a total of $\prod_{i=0}^{r-1} d_i$

elements. As an example, rank-1 tensors are equivalent to vectors, while rank-2 tensors are isomorphic to matrices.

The tensor indices can be connected, which indicates a *tensor contraction* operation. This multiplies two tensors similar to matrix multiplication, resulting in a new tensor. E.g., two tensors A_{ij} and B_{klm} can be connected on the first and second index respectively, creating a tensor $C_{jkm} = \sum_i A_{ij} B_{kim}$. Connecting multiple tensors across their indices creates a **tensor network**, which is transformed by repeatedly contracting the individual tensors in a given *contraction order*. In practice, some orders have lower computational cost than others, which is why this representation is more flexible. The paired lines are called *closed indices*, while the unpaired ones are *open indices*. An example tensor network is shown on Fig. 3.

E. Matrix product states

Among various tensor network representations of quantum circuits, there is a particularly useful way to encode a state with the memory usage directly related to quantum entanglement in the system. This is achieved by performing a repeated **singular value decomposition (SVD)** operation on the statevector. The number of non-zero singular values determines how large the state tensors need to be. Overall, the final tensor network can be thought of as a product of matrices labelled by statevector indices, also known as *physical indices*. Meanwhile, the bonds that connect the matrices are known as *virtual indices*. This construct is also known as **matrix product states (MPS)** [18].

In practice, the MPS is rarely formed via decomposition due to the exponential nature of the statevector, which would make the SVD largely inefficient, as its complexity is cubic in matrix dimensions [21]. Some MPS are trivial to construct, for example for the $|0\rangle$ state, all matrices are 1×1, with entry 1 for matrices labelled 0, and entry 0 for matrices numbered 1. In fact, any individual bitstring state can be formed this way, and the size of the matrices implies that their maximum **bond dimension** is 1. For more complex states, it is possible to use *finite automata* to determine all matrix elements [22].

MPS can be directly evolved by applying tensors, with the caveat that all consecutive sites between the targets need to be recontracted, and decomposed again, which can be costly for longer-range interactions. As an alternative, an operator can be decomposed itself into **matrix product operators (MPO)** equivalently to how MPS is formed. Again, this may be costly, and it is often more efficient to construct the MPO directly from the operator form, by considering how it modifies individual sites.

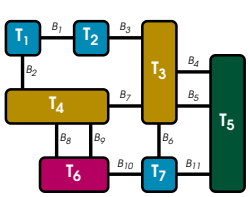

Fig. 3. Example network with 7 tensors and 11 bonds.

Depending on the circuit and the input state, the size of the site matrices can grow arbitrarily, which is undesirable. To prevent this, we can use *singular value truncation*, where the rows/columns corresponding to the lowest singular values are rejected. Since the SVD usually returns sorted singular values, this is trivial to implement. Consequently, the information loss from disregarding some components is minimised.

Contracting two MPS with each other (where the second MPS is conjugated) returns an *overlap* of two statevectors. Taking an overlap of the MPS with itself calculates the squared *norm*, which should be 1 for non-approximated states. If the norm changes, e.g. due to truncation, the MPS can be *renormalised* by dividing each site by the same factor. MPS can also be combined with itself by taking a tensor product, which results in a *density matrix*.

In general, there is no restriction to the form of the MPS, and each matrix can have arbitrary elements, as long as the product yields the original statevector. However, evolving an arbitrary MPS is inefficient and might lead to linearly dependent components, and SVDs with all singular values being equal. This is undesirable for truncation, as the accuracy loss is no longer sorted. To remedy that, the MPS should be converted to a **canonical form**, which is achieved by repeatedly decomposing and multiplying site tensors. The goal is to make all matrices on one hand side unitary, which means that their overlap returns an identity. As a side effect, this helps spread out the entanglement throughout the system. In most cases, the required form is *mixed canonical*, where there is some center site surrounded by unitaries on both sides. MPO can also be converted to a canonical form, and ideally, before contracting an MPS-MPO pair, the MPS should have the canonical centre at the first site that the MPO is applied to, while the latter should be canonical to the right.

F. Existing libraries

Many tensor network libraries are available, so the focus here will be libraries used in the HPC setting and specifically for emulation of quantum computers. *ITensor* is a frequently-used framework for solving many-body problems, which can be leveraged to represent circuits. It has two implementations in C++ in Julia, where the former has been discontinued, and the latter offers GPU acceleration [9]. *Quimb* is a high-performance Python package with extended functionality, which suppports some distributed operations via PETSc/SLEPc backends [23]. NVIDIA also made a quantum tensor network ecosystem, based on *cuTensorNet* and *cuQuantum*, which offers GPU acceleration and slice-based tensor network distribution [13]. Another popular framework, which was originally made for quantum chemistry problems, is *Cyclops Tensor Framework (CTF)*. It offers a powerful tool set for efficient dense and sparse tensor operations, and has an interface to ScaLAPACK routines [11]. Finally, ExaTN is an exascale project for solving tensor network problems on large heterogeneous clusters, including GPU support. It is built on top of *TNQVM*, which is an extensive ecosystem of interdependent libraries, many of which are required to compile and

run it [12]. None of the mentioned libraries appears to offer a way to distribute individual tensors besides the slice-based approaches, which are executed in the wider tensor network setting – this is the gap that we strive to fill.

III. Implementation

Quantum tensor network hub (QTNH) is a library for large-scale dense tensor network contraction with distributed individual tensors. The main focus is increasing the maximum size of tensors stored in the network, as this can correspond to the simulation accuracy. Here, we describe the structure and capabilities of the library, justified by the consideration taken during implementation.

A. Tensors

Multidimensional objects like tensors are complex to implement efficiently, as the order of axis iteration can be arbitrary, which entails random memory accesses. In QTNH, we decided to use a *flat contiguous data layout*, with *row-major (lexicographic) ordering*, such that indices on the right increase faster. This means that contiguous data accesses only occur for the rightmost index.

Tensors can be **distributed** across multiple MPI ranks by scattering leftmost *local indices*, which converts them to *distributed indices*. The values of distributed indices are used to label the rank that holds given local elements, also in the row-major order. To picture the tensor dimensions, an *index tuple* is used, with an optional semicolon to separate distributed and local indices, e.g. $(2, 3; 4, 2)$ is a rank-4 tensor with distributed size of 6 and local size of 8.

Tensors can also be **broadcast** with three parameters:

1) *stretch* (str) – determines on how many consecutive ranks each local tensor is repeated.
2) *cycles* (cyc) – indicates how many times the global tensor structure is repeated.
3) *offset* (off) – points at the first rank the tensor is on.

Therefore, a tensor spans $str \cdot cyc \cdot N_d$ ranks, where N_d is the distributed size of a single tensor instance, and begins at rank off. The additional parameters are useful for both aligning related tensors, and uncoupling independent tensors – the former prevents unnecessary synchronisation, while the latter can enable parallel operations, provided globally blocking operations are not used. The distribution pattern for both scatter and broadcast features is summarised in Fig. 4.

Index permutation/transpose is a fundamental tensor operation that rearranges the elements to match a permuted index tuple. In a general case, this routine involves irregular all-to-all communication, when distributed indices are exchanged with the local ones. Two communication examples are presented in Fig. 5. In QTNH, it has been implemented with a single `MPI_Alltoallv` call, which communicates the elements based on a complex multi-nested MPI datatype, where each layer implements a contiguous type and resizes it. The number of layers can be relatively large, and a limitation of the MPICH implementation was encountered, as it internally supports up to 15 nested datatypes. This was partially avoided by combining fixed-size-layers together, which should cover all but most irregular permutations.

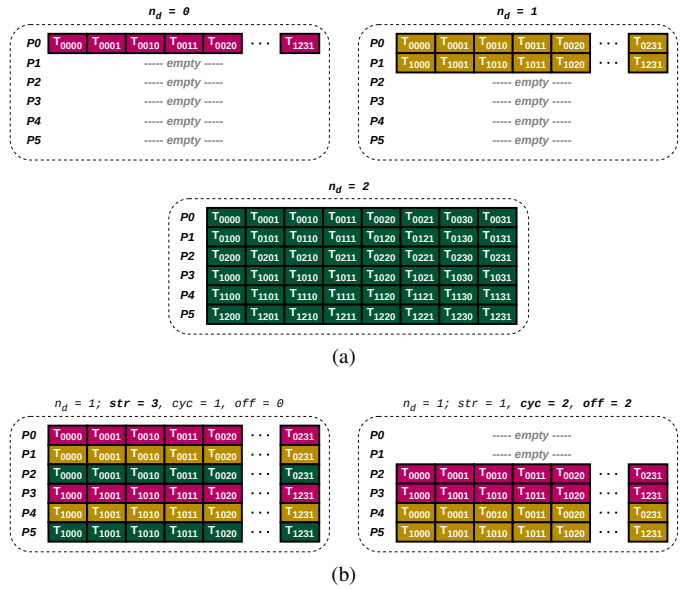

Fig. 4. Tensor distribution in QTNH of a $(2, 3, 4, 2)$ tensor. Fig. 4a shows the process of scattering the first two indices. Fig. 4b visualises different broadcast patterns – here each colour indicates a different copy of the tensor.

The tensors are currently divided into four main categories:

1) **Dense tensors** – store all elements in a vector.
2) **Symmetric tensors** – same as dense tensors, but the dimensions of input and output dimensions must be identical, and have the same distribution. In practice, this means that both distributed and local dimensions are split in half.
3) **Diagonal tensors** – symmetric tensors that only store diagonal elements, for which the input and output indices are equal. All other elements are implicitly zero.
4) **Special tensors** – regular structure tensors, like SWAP or identity, were the elements can be directly computed from their location.

All tensors can be converted to a dense tensor, and sometimes to other categories, depending on their inheritance tree.

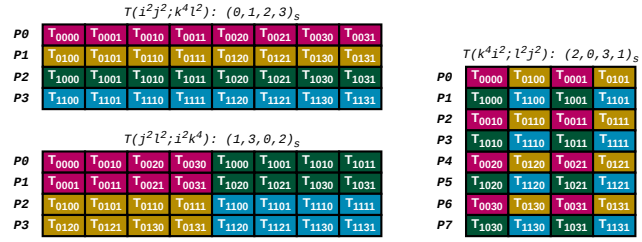

Fig. 5. Examples of permuting indices of a $(2; 2, 4, 2)$ tensor. Moving the 4-dimensional local index to the distributed position is an *asymmetric permutation* and requires more MPI ranks than the original tensor.

B. ScaLAPACK Integration

Functions that determine the distribution pattern of tensors were implemented manually using only MPI. However, more complex operations such as contraction and decomposition are tackled with an external tool, ScaLAPACK. It is a high-performance distributed-memory dense linear algebra library [24].

ScaLAPACK stores matrices as block-cyclic 2-dimensional arrays, and in column-major format, common in Fortran. However, the distributed blocks are by default indexed as row-major. Therefore, before calling any routines, it is necessary to convert between the QTNH and ScaLAPACK formats – which is handled using index permutation. To determine the permutation needed to create a block-cyclic matrix, the following notation is used:

$$T^{\{i_c\}\{\underline{i}_d\}\{i_b\}}_{\{j_c\}\{\underline{j}_d\}\{j_b\}}$$

Upper indices are used for rows, while lower indices for columns. In addition, indices are split into groups, where c are cyclic indices, d are distributed indices and b are block indices. In the row-major tuple format introduced in section III-A, this is equivalent to the following:

$$\Big(\{\underline{i}_d\}\{\underline{j}_d\};\{j_c\}\{j_b\}\{i_c\}\{i_b\}\Big)$$

where the local indices are inverted due to row-major to column-major conversion. The permutation tuple depends then on what the original representation was.

Tensor contraction can be converted to matrix multiplication by treating all contracted dimensions as column indices of the first operand, and row indices of the second operand. Distributed dimensions are used as block indices, while local dimensions can either label cycles or local elements within a current block-cycle. The contraction routine is `PZGEMM` for parallel complex general matrix-matrix multiplication.

Singular value decomposition is handled using the `PZGESVD` routine for parallel complex general SVD. It requires matrices of similar form to GEMM, with an additional restriction that local contiguous blocks need to be square. The SVD in ScaLAPACK uses an additional work array, whose size is estimated using the same routine as a query.

C. Tensor Networks

Tensors are stored in a *tensor network*, together with *bonds*, which are used to specify how the tensors are connected. While the typical goal of tensor networks is to map it to a single tensor, in QTNH, there are four distinct operations to transform a network by mapping tensors and tensor pairs:

1) **Rebcast** ($T \to T$) transfers/broadcasts tensor elements to modify the distribution pattern.
2) **Contract** ($T, T \to T$) combines two tensors into one, summing over the bonds that connect them.
3) **Decompose** ($T \to T, T$) splits a tensor into two and creates additional bonds connecting them.
4) **Truncate** ($T, T \to T, T$) removes elements in two tensors, while resizing bonds between them.

In addition, the tensor operations like index swapping/permutation and scattering is handled by inserting special tensors into the network. This is because these operations can be directly represented with tensors, e.g. scattering a local index is equivalent to an identity tensor with a distributed output index. This is very useful because of an important restriction that tensor network bonds can only connect indices of the same type, i.e. local-local and distributed-distributed.

D. Matrix product states

An MPS combined with MPOs is an example of a tensor network that uses a specific network *factorisation*. As a result, it is always expected to have a preserved form, which requires additional operations, such as:

- Apply raw quantum gate to MPS
- Apply MPO to MPS
- Move canonical center
- Compute overlap with other MPS
- Renormalise
- Sample from selected sites

They can be built on top of the basic four operations introduced in section III-C.

Currently, QTNH implements a *fixed bond dimension MPS*, in which the states have constant size, and are padded with zeros. It is less efficient than variable dimension, but also easier to keep track of. When bond dimension gets saturated, all excessive singular values are truncated in an ascending order from the smallest one.

To make room for more singular values, the bond dimension is distributed. Therefore, for an MPS with physical dimension $d = 2$ and virtual dimension χ, the corresponding tensor has the following shape:

$$(\chi_d, \chi_d; d, \chi_l, \chi_l)$$

such that $\chi = \chi_d \chi_l$ defines the split between distributed and local virtual dimensions.

E. Benchmarking circuits

This paper uses two algorithms for benchmarking, implemented in various forms. The first one is the QFT, which is known for introducing little entanglement [19]. The other one is the random circuit sampling (RCS) algorithm used by Google, whose sole purpose is to saturate the entanglement as quickly as possible [20]. Thus, two boundary cases were chosen to show how the library handles different scenarios.

1) QFT algorithm: The QFT is a great demonstration how matrix product states can change the emulation performance. First, a standard statevector-like tensor network has been implemented, in line with Fig. 1, where each gate is a separate tensor, and the contraction order goes identically to the gate application order. To distribute this, the first d horizontal lines in the circuit diagram represent distributed indices, both for the state and the connected gates.

The second tensor network leverages the MPO representation to build circuit operators. They are still applied directly

to the full state, without using MPS. The controlled gate operators can be constructed using the following MPOs:

$$\begin{pmatrix}\hat{\Pi}_0 & \hat{\Pi}_1\end{pmatrix}\begin{pmatrix}\hat{I} & 0\\ 0 & \hat{P}_2\end{pmatrix}\cdots\begin{pmatrix}\hat{I} & 0\\ 0 & \hat{P}_{k-1}\end{pmatrix}\begin{pmatrix}\hat{I}\\ \hat{P}_k\end{pmatrix}$$

where $\hat{\Pi}_k$ is a projector onto state $|k\rangle$, while $\hat{P}_k$ represents phase shift by $\frac{2\pi}{2^k}$. This representation combines all phase shifts per control into a single MPO [19]. In addition, all Hadamard gates can also be absorbed into the MPOs. The final circuit is shown in Fig. 6a. The contraction order first combines the MPO tensors into groups, and afterwards, each layer of tensors is contracted with the state in sequence.

Finally, the third implementation of the QFT is based on the MPS in place of the statevector. The controlled MPO layers are constructed the same as above, and the Hadamard gates are applied separately. SWAP gates at the end can also be represented as MPOs, even though they are optional in this case. The MPS state can be randomly initialised to a given maximum starting bond dimension, and renormalised. The whole network is shown in Fig. 7.

2) RCS algorithm: In the random circuit sampling, the only MPO needed is for the entangling layer, as all single-qubit gates can be applied directly to the MPS. An $fSim$ gate can be made into an MPO with arbitrary interaction length by considering the following matrix product:

$$\begin{pmatrix}\hat{\Pi}_0 & -i\hat{S}_- & -i\hat{S}_+ & e^{i\pi/6}\hat{\Pi}_1\end{pmatrix}\begin{pmatrix}\hat{I} & 0 & 0 & 0\\ 0 & \hat{I} & 0 & 0\\ 0 & 0 & \hat{I} & 0\\ 0 & 0 & 0 & \hat{I}\end{pmatrix}^k\begin{pmatrix}\hat{\Pi}_0\\ \hat{S}_+\\ \hat{S}_-\\ \hat{\Pi}_1\end{pmatrix}$$

where k stands for the number of sites between the target sites, and $\hat{S}_-$, $\hat{S}_+$ are lowering/raising operators, i.e. $|0\rangle\langle 1|$, $|1\rangle\langle 0|$ respectively. Thus, an $fSim$ MPO has bond dimension of 4.

The entangling layers are applied in an $ABCDCDAB$ pattern, where A/B are across rows, and C/D are across columns. If qubits are stored in the row-major order, this means that A and B patterns can be applied in parallel, while C and D need to perform each operation individually, which causes much larger entanglement to build up, as a product of multiple MPOs is effectively applied. A diagram of the RCS MPS tensor network is shown in Fig. 8

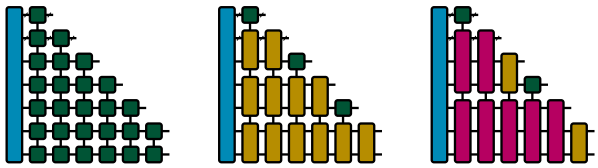

(a) (b) (c)

Fig. 6. 7-qubit QFT treated as a tensor network with custom contraction order. The operator tensors are constructed using the MPO formalism, which combines all controlled phase operators into a single layer per upper control. The contraction order goes up-to-down and left-to-right, and horizontal indices in the upper part are distributed to minimise communication. Fig. 6a shows the original network, Fig. 6b combines operators in groups of two, while Fig. 6c uses groups of three.

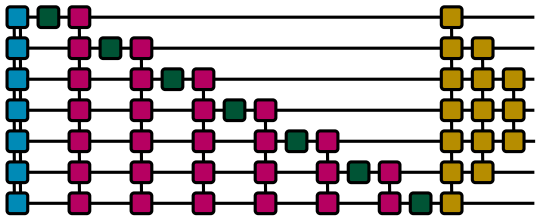

Fig. 7. Quantum Fourier transform as an MPS. All phase gates with the same control have been converted to a single MPO.

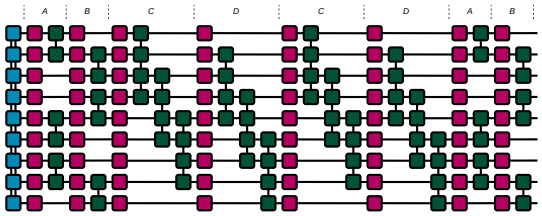

Fig. 8. 3×3 RCS circuit converted to an MPS. Magenta layers are random single-qubit gates, while dark green layers implement the fSim operation according to one of the four patterns.

IV. Results

This section covers experiments that demonstrate the capabilities of QTNH. As highlighted before, the main focus is not performance, but the ability to store large tensors, and its impact on the result quality. In addition, the general benefits of tensor networks, such as flexible contraction order and MPS factorisation, are explored.

A. QFT scaling

As described in section III-E, the QFT was implemented using three different approaches – statevector-inspired network, MPO-inspired network and MPS. In the first two implementations, a number of qubits at the top is treated as distributed qubits, which means all horizontal wires between tensors above the split are scattered. All other indices are local.

Fig. 9 shows weak scaling of the statevector approach, such that the number of local qubits (n_l) is fixed per colour. The number of distributed qubits (n_d) is plotted against the total emulation runtime. In a perfect case, the runtime should double per added local qubit, and scale quadratically with total qubits $n = n_l + n_d$, due to the nature of the algorithm. As shown in the figure, both predictions are close, however, the slope is greater than 2 and changes for more qubits – this is likely because a single node can hold at most 7 distributed qubits (128 cores), and afterwards the communication cost becomes a bottleneck. Each colour on the plot starts at 4 distributed qubits, as 16 ranks are already required for gate distribution.

The MPO-inspired network is made to demonstrate that different contraction orders can speed up the runtime. Before applying the operator tensors into the state, they are first combined into larger tensors. Despite slightly increasing the problem complexity, this allows ScaLAPACK to perform the contraction routines more efficiently, as less processing is required. Consequently, moderately expanding the size of

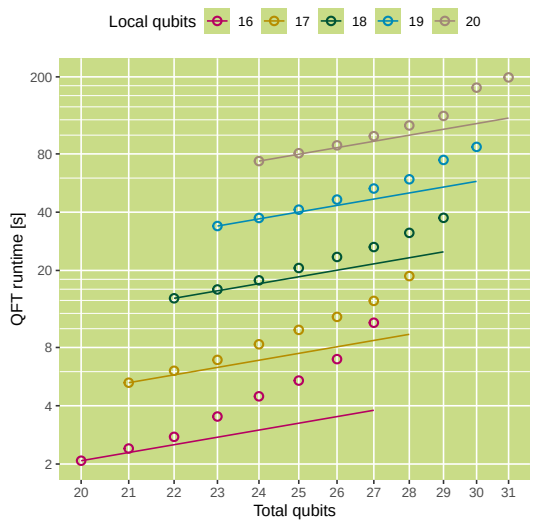

Fig. 9. Statevector-inspired QFT weak scaling on a double-log plot. The spacing should be comparable, as each local qubit doubles the work. The slopes are related to the power of runtime scaling, as we expect $y \sim x^{\alpha}$, where ideally $\alpha = 2$, as indicated by the straight lines. On the plot above, the initial α ranges between 2.3 and 3.0.

intermediate tensors can help solve the problem faster to some extent. This is demonstrated in Fig. 10, where groups of up to 5 tensors are created. The maximum size of the group depends on the number of distributed qubits, as this also determines how many ranks are used. We can see that after fixing n_l and n_d, the runtime decreases as the group size grows, but the improvement stops around 4–5 tensors.

Finally, the MPS approach is run for the $|0\rangle$ input state, for which the difference between the statevector approach and the MPS is the clearest, as the bond dimension should stay 1 throughout the emulation. For practical reasons, the bond dimensions are set to $\chi_d = 1$ and $\chi_l = 2$ to enable an additional degree of freedom. Consequently, only 1 rank needs to be used. The result is left in the MPS format at the end, as otherwise the program would run out of memory. The time scaling is plotted in Fig. 11. As expected, the runtimes follow an almost ideal quadratic function, and up to a thousand qubits can be emulated within reasonable time.

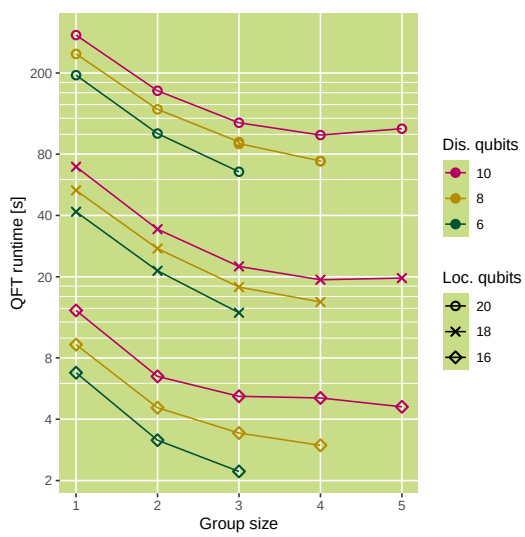

Fig. 10. Custom MPO-inspired tensor network QFT runtimes for different contraction orders. The maximum group size cannot exceed $\frac{1}{2}n_d$, as the run can support at most n_d distributed indices, and the operator tensors have indices on both sides.

B. QFT MPS bond dimension

The next set of experiments focuses on the MPS distribution, evaluating how changing the bond dimension impacts the performance and accuracy. The $|0\rangle$ input QFT can be used here, as the representation enforces a fixed bond dimension, which is padded with zeros in this case. The MPS uses the format defined in section III-D. Here, the distributed bond χ_d does not have to be power-of-two, but the distributed size should allow uniform problem paritioning.

The results are displayed in Fig. 12, where each colour fixes χ_l and varies χ_d. There are two factors influencing the scaling – MPS-MPO products and the SVDs. As χ_d increases, the former is expected to be $\mathcal{O}(\chi_d^2)$, which is also how the number of involved processes grows. Meanwhile, the SVD is $\mathcal{O}(\chi_d^3)$, so the ideal scaling per process is χ_d [21]. However, both operations are tightly coupled, and the communication overhead is likely to be significant. The values of χ_d are not limited to powers of two, but it is preferable that they divide evenly across the nodes. We can see that the plots per colour don't follow a straight line, and power-of-two values scale better than other χ_d, likely due to load balancing.

A similar setup can be used to measure the strong scaling, such that the total χ is fixed, and the split between the distributed and virtual dimensions changes. The results, together with the parallel efficiency, are presented in Fig. 13. With each double χ_d, the number of ranks is quadrupled. There is an initial benefit of parallelisation, but the efficiency quickly plummets. This could be due to coupling in routines like the SVD, as well as the performance of ScaLAPACK with small local objects. Indeed, the speedup is noticeable for the first few

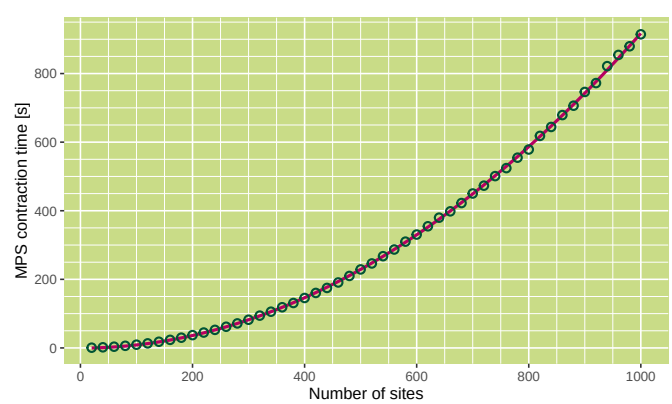

Fig. 11. MPS QFT runtime for $|0\rangle$ input state. The magenta line fits a quadratic function to the results.

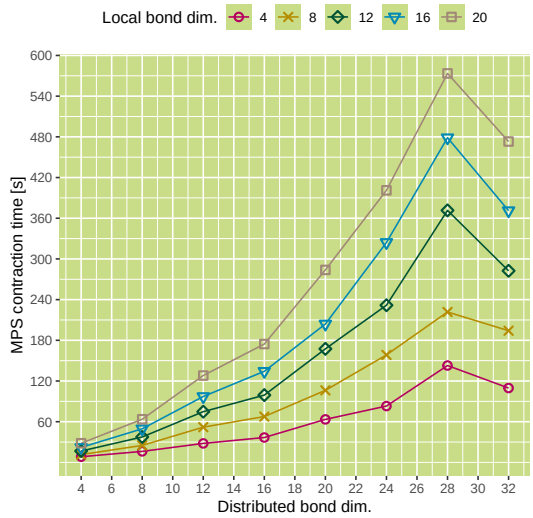

Fig. 12. QFT MPS contraction time scaling with increasing maximum bond dimension. For χ_d that are not powers of 2, the workload is split evenly between the nodes.

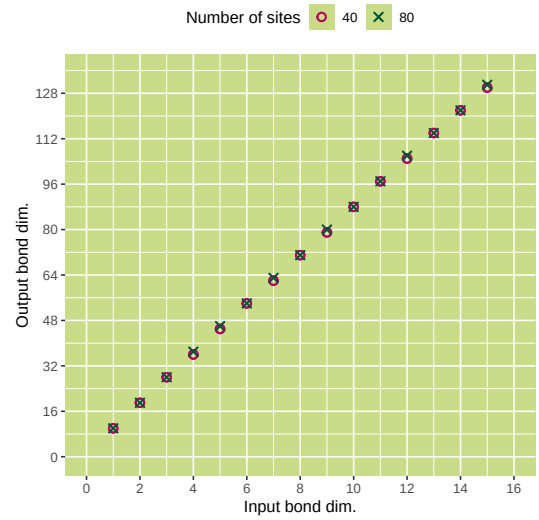

Fig. 14. MPS QFT input vs output bond dimension for two different MPS sizes. The input is initialised to a random MPS with a given bond dimension.

points, so distributing some calculations can be advantagous, especially for larger runs. Nevertheless, keeping local bonds relatively large should be prioritised.

For the next experiment, we initialise a random MPS with predefined bond dimensions. This is achieved by filling parts of the MPS with random complex values, and then renormalising to satisfy the probability constraint. The input state is fed into the QFT and transformed, while keeping track of the non-zero bond dimension. It turns out that the output MPS bond size is $\sim$8 times larger than the input state, regardless of the size of the system. The relation is shown in Fig. 14.

The total χ can also be varied, such that it is lower than the bond size of the output state. This is helpful to estimate how much accuracy is lost after performing the unavoidable truncation. There are two methods to measure the accuracy – by checking the norm, which should always decrease after truncation, and by taking the overlap between the smaller MPS and the ideal one. The latter method is likely to be more reliable, as it directly uses the correct output. Both accuracy metrics are present in Tab. I, for two random MPS inputs, one with $\chi = 16$, while the other one is with $\chi = 32$.

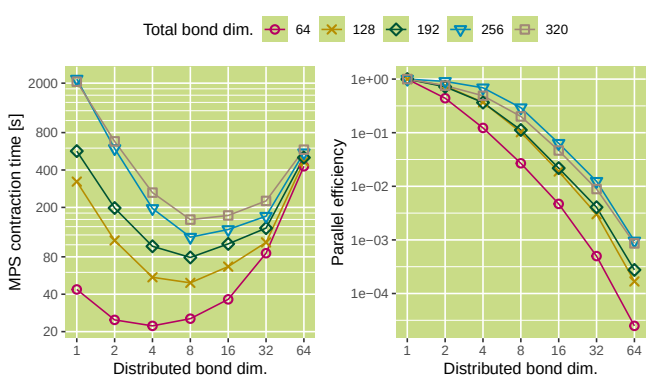

Fig. 13. MPS QFT strong scaling for fixed values of $\chi = \chi_d \chi_l$. When χ_d is doubled, the number of ranks required increases four times. The plot on the left shows runtime scaling , while the plot on the right parallel efficiency, both wrt. $\chi_d = 1$.

C. RCS MPS accuracy

In case of the random circuit sampling algorithm, the output accuracy is expected to deteriorate quickly for larger qubit grid sizes. Therefore, the overlap accuracy metric will be more and more difficult to compute, and instead norm accuracy has to be used. In Tab. II, we compare both metric for a 4×4 grid with depth 8, as it is still possible to compute an ideal result within reasonable time. Similarly to the QFT, the output accuracy for both metrics appears to stay consistent, however, it is important to note that the percent difference slowly increases, reaching about 5–10% for lower bond dimensions. As a result, the norm can be treated as an approximation of the overlap. This is likely due to the fact that if truncation happens in an arbitrary direction, it should on average decrease every component to the same degree, including the direction of the ideal result.

TABLE I
QFT ACCURACY METRICS

Chi	256	128	64	32	16
Overlap	1.0000	1.0000	0.9998	0.9442	0.4901
Norm	1.0000	1.0000	0.9998	0.9393	0.4866

[a] Input bond dimension: $\chi = 16$.

Chi	512	256	128	64	32
Overlap	1.0000	1.0000	0.9998	0.9482	0.5191
Norm	1.0000	1.0000	0.9998	0.9426	0.5138

[b] Input bond dimension: $\chi = 32$.

TABLE II
RCS ACCURACY METRICS
(4×4 QUBITS, 8 LAYERS)

Chi	512	256	128	64	32	16	8
Overlap	1.000	0.842	0.452	0.212	0.108	0.057	0.041
Norm	1.000	0.839	0.454	0.204	0.095	0.052	0.043
Diff.	0.000	0.003	0.002	0.008	0.013	0.005	0.002
Rel.	0.000	0.004	0.004	0.038	0.137	0.096	0.049

[a] *Diff.* – absolute difference ($|\text{overlap} - \text{norm}|$).
[b] *Rel.* – relative difference ($\text{diff}/\min(\text{overlap}, \text{norm})$).

The RCS accuracy experiment has been performed for four square grids between 4 and 7 qubits in each direction, with up to $\chi = 1024$. The depth of each circuit is 8, to allow one full entangling cycle to complete. The results are presented in Fig. 15. It is clear that larger grids are much more difficult to emulate, where for the 7×7 grid, the norm barely raises over 10^{-3}. This is because a linear change in the number of qubit exponentially increases the maximum entanglement, and hence, the accuracy is expected to drop in a similar manner.

The largest experiment on the 7×7 grid has also been independently completed – spanning 18 nodes and 2304 ranks of ARCHER2, and taking 10.5 hours to finish. The bond dimensions used were $\chi_d = 48$, $\chi_l = 48$, $\chi = 2304$, and the final accuracy was $2.5 \cdot 10^{-3}$.

V. Future Work

This paper offered an overview of the unique features that the QTNH library implements. However, plenty of work is still required to make it faster and easier to use.

While the library theoretically supports different tensor operations in parallel, it is not possible to leverage this with enabled ScaLAPACK support. This is because ScaLAPACK uses globally blocking collectives in its distributed grid initialisation, more specifically `MPI_Comm_create`. QTNH prevents this by using `MPI_Comm_group_create` instead, which synchronises only the involved group – which might be possible to utilise in ScaLAPACK as well.

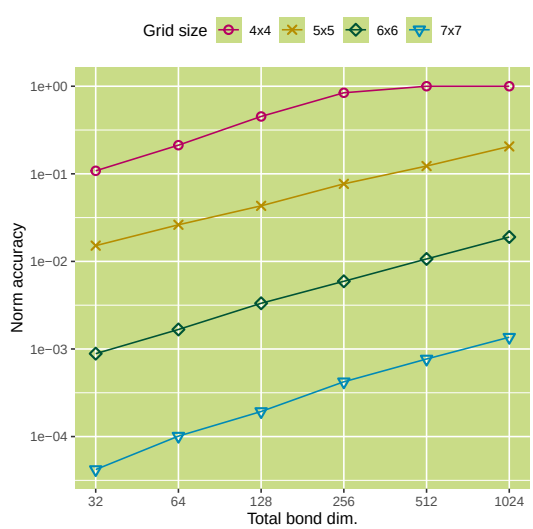

Fig. 15. RCS MPS accuracy scaling wiht increasing bond dimension for different qubit grid sizes.

A number of additional optimisations can also be implemented. On the algorithm level, a variable MPS would be helpful to both reduce the memory footprint and accelerate the computation for systems with small entanglement. On a lower level, it might be possible to get more performance from individual routines by investigating the impact of different distribution patterns. This could potentially bring down the communication cost and the number of permutations required.

Finally, one of the reasons that QTNH is not yet competitive in terms of performance with other HPC libraries is lack of internal optimisers and accelerator support. Contraction order optimisation is a part of packages like CTF, cuQuantum or Quimb, and for QTNH, it would be helpful to include an operation order optimiser, which would also encompass other tensor network operations. Moreover, GPU support can be added for accelerating local contractions. Both of those problems could be solved by switching to either CTF or cuTensorNet as backend, since in principle those libraries operate on a lower level, and it might be possible to incorporate the distribution pattern used by QTNH within their environments. However, this would likely negatively impact portability, which is a big part of the library's design.

VI. Conclusion

We presented *Quantum Tensor Network Hub (QTNH)* – a portable distributed tensor network library that proposes a novel distribution pattern at the level of individual tensors, together with a fixed set of operations to modify them. In contrast to circuit slicing, this approach offers direct access to contraction results at all times. Moreover, it unlocks multiple layers of parallelism, from single tensors, to entire tensor networks. The library utilises MPI and ScaLAPACK to distribute and modify the tensors.

A tensor network together with a particular sequence of operations can be used to implement more complex computational tasks, such as the emulation of quantum computers. It was demonstrated that this formalism can be employed to solve the same problem using multiple approaches – in particular, we proposed a large-scale MPS tensor factorisation technique with distributed entanglement storage. We believe that this library can become an alternative to existing tools, offering an easy-to-use and flexible interface to tensor network computations.

Acknowledgment

This work used the ARCHER2 UK National Supercomputing Service (https://www.archer2.ac.uk). This work was supported by the Engineering and Physical Sciences Research Council grant number EP/T517884/1.

References

[1] A. M. Childs and J. Goldstone, "Spatial search by quantum walk," *Phys. Rev. A*, vol. 70, p. 022 314, 2 Aug. 2004. DOI: 10.1103/PhysRevA.70.022314. [Online]. Available: https://link.aps.org/doi/10.1103/PhysRevA.70.022314.

[2] P. W. Shor, "Algorithms for quantum computation: Discrete logarithms and factoring," 1994. DOI: 10.1109/SFCS.1994.365700.

[3] J. R. McClean *et al.*, "The theory of variational hybrid quantum-classical algorithms," *New Journal of Physics*, vol. 18, no. 2, p. 023 023, Feb. 2016. DOI: 10.1088/1367-2630/18/2/023023. [Online]. Available: https://dx.doi.org/10.1088/1367-2630/18/2/023023.

[4] Google Quantum AI *et al.*, "Quantum error correction below the surface code threshold," *Nature*, vol. 638, pp. 920–926, Feb. 2025, ISSN: 0028-0836. DOI: 10.3929/ethz-b-000723955.

[5] T. Häner *et al.*, "High performance emulation of quantum circuits," in *SC '16: Proceedings of the International Conference for High Performance Computing, Networking, Storage and Analysis*, 2016, pp. 866–874. DOI: 10.1109/SC.2016.73.

[6] I. L. Markov and Y. Shi, "Simulating quantum computation by contracting tensor networks," *SIAM Journal on Computing*, vol. 38, no. 3, pp. 963–981, 2008. DOI: 10.1137/050644756. eprint: https://doi.org/10.1137/050644756.

[7] F. Pan and P. Zhang, "Simulation of quantum circuits using the big-batch tensor network method," *Physical Review Letters*, vol. 128, 3 Jan. 2022, ISSN: 10797114. DOI: 10.1103/PhysRevLett.128.030501.

[8] Y. Zhou, E. M. Stoudenmire, and X. Waintal, "What limits the simulation of quantum computers?" *Physical Review X*, vol. 10, no. 4, p. 041 038, Nov. 2020, ISSN: 2160-3308. DOI: 10.1103/PhysRevX.10.041038.

[9] M. Fishman, S. White, and E. M. Stoudenmire, "The ITensor Software Library for Tensor Network Calculations," *SciPost Physics Codebases*, p. 004, Aug. 2022, ISSN: 2949-804X. DOI: 10.21468/SciPostPhysCodeb.4. (visited on 11/07/2024).

[10] K. Z. Ibrahim *et al.*, "Analysis and tuning of libtensor framework on multicore architectures," in *2014 21st International Conference on High Performance Computing (HiPC)*, Dec. 2014, pp. 1–10. DOI: 10.1109/HiPC.2014.7116881. (visited on 04/28/2025).

[11] E. Solomonik *et al.*, "A massively parallel tensor contraction framework for coupled-cluster computations," *Journal of Parallel and Distributed Computing*, Domain-Specific Languages and High-Level Frameworks for High-Performance Computing, vol. 74, no. 12, pp. 3176–3190, Dec. 2014, ISSN: 0743-7315. DOI: 10.1016/j.jpdc.2014.06.002. (visited on 04/28/2025).

[12] D. I. Lyakh *et al.*, "ExaTN: Scalable GPU-Accelerated High-Performance Processing of General Tensor Networks at Exascale," *Frontiers in Applied Mathematics and Statistics*, vol. 8, Jul. 2022, ISSN: 2297-4687. DOI: 10.3389/fams.2022.838601. (visited on 04/28/2025).

[13] H. Bayraktar *et al.*, "Cuquantum sdk: A high-performance library for accelerating quantum science," in *2023 IEEE International Conference on Quantum Computing and Engineering (QCE)*, vol. 01, 2023, pp. 1050–1061. DOI: 10.1109/QCE57702.2023.00119.

[14] J. Adamski, *Jjacobx/qtnh: Vcluster25*, version vcluster25, May 2025. DOI: 10.5281/zenodo.15374616. [Online]. Available: https://doi.org/10.5281/zenodo.15374616.

[15] P. Ferrero-Roza, J. A. Moríñigo, and F. Terragni, "Strong Scaling of The SVD Algorithm For HPC Science: A Petsc-Based Approach," in *2023 Winter Simulation Conference (WSC)*, Dec. 2023, pp. 2872–2883. DOI: 10.1109/WSC60868.2023.10407904. (visited on 04/28/2025).

[16] M. A. Nielsen and I. L. Chuang, *Quantum Computation and Quantum Information*, 10th. Cambridge University Press, Jun. 2012, ISBN: 9781107002173. DOI: 10.1017/CBO9780511976667.

[17] J. Biamonte, "Lectures on quantum tensor networks," *arXiv preprint*, Dec. 2019. DOI: 10.48550/ARXIV.1912.10049. [Online]. Available: http://arxiv.org/abs/1912.10049.

[18] U. Schollwöck, "The density-matrix renormalization group in the age of matrix product states," *Annals of Physics*, January 2011 Special Issue, vol. 326, no. 1, pp. 96–192, Jan. 2011, ISSN: 0003-4916. DOI: 10.1016/j.aop.2010.09.012. (visited on 11/07/2024).

[19] J. Chen, E. Stoudenmire, and S. R. White, "Quantum Fourier Transform Has Small Entanglement," *PRX Quantum*, vol. 4, no. 4, p. 040 318, Oct. 2023. DOI: 10.1103/PRXQuantum.4.040318. (visited on 11/07/2024).

[20] F. Arute *et al.*, "Quantum supremacy using a programmable superconducting processor," *Nature*, vol. 574, no. 7779, pp. 505–510, Oct. 2019, ISSN: 1476-4687. DOI: 10.1038/s41586-019-1666-5. (visited on 11/07/2024).

[21] J. Demmel, "6. Singular Value Decomposition," in *Templates for the Solution of Algebraic Eigenvalue Problems*, ser. Software, Environments, and Tools, Society for Industrial and Applied Mathematics, Jan. 2000, pp. 135–147, ISBN: 978-0-89871-471-5. DOI: 10.1137/1.9780898719581.ch6. (visited on 05/02/2025).

[22] G. M. Crosswhite and D. Bacon, "Finite automata for caching in matrix product algorithms," *Physical Review A*, vol. 78, no. 1, p. 012 356, Jul. 2008. DOI: 10.1103/PhysRevA.78.012356. (visited on 05/01/2025).

[23] J. Gray, "Quimb: A python package for quantum information and many-body calculations," *Journal of Open Source Software*, vol. 3, no. 29, p. 819, Sep. 2018,

ISSN: 2475-9066. DOI: 10.21105/joss.00819. (visited on 04/28/2025).

[24] L. S. Blackford *et al.*, *ScaLAPACK Users' Guide*. Society for Industrial and Applied Mathematics, 1997. DOI: 10.1137/1.9780898719642. eprint: https://epubs.siam.org/doi/pdf/10.1137/1.9780898719642.